and Prof. Shuangyin Wang (shuangyinwang@hnu.edu.cn)

Reactivity and Durability of TiO_2 Photoanodes with Dominant High-Energy (211) Facets

Yanhong Lyu[a], Jianyun Zheng[a*], Aibin Huang[b,c], Huaijuan Zhou[d], San Ping Jiang[e], Shuangyin Wang[a*]

[a.] *State Key Laboratory of Chem/Bio-Sensing and Chemometrics, College of Chemistry and Chemical Engineering, Hunan University, Changsha 410082, Hunan, China.*

[b.] *State Key Laboratory of High Performance Ceramics and Superfine Microstructure, Shanghai Institute of Ceramics, Chinese Academy of Sciences, Shanghai 200050, China.*

[c.] *University of Chinese Academy of Sciences, Beijing, 100049, China.*

[d.] *Advanced Research Institute of Multidisciplinary Sciences, Beijing Institute of Technology, Beijing 100081, China*

[e.] *WA School of Mines: Minerals, Energy and Chemical Engineering, Curtin University, Perth, WA 6102, Australia*

∗ Corresponding Author: Prof. Jianyun Zheng (jyzheng@hnu.edu.cn)

Preparation of bulky TiO_2 photoanode

Fluorine-doped tin oxide glass (FTO) with an area of 100 and 2 cm^2, single-side-polished p-type Si (p-Si) wafers with a resistivity of 1-10 Ω cm, Ti foils with an area of 2 cm^2, indium tin oxide glass (ITO) with an area of 2 cm^2 area and BK7 glass with an area of 4 cm^2 were applied as the substrates and orderly cleaned via using ultrasonic baths in alkaline solution/acetone/acid solution, ethanol and deionized water. These clean and dry substrates were loaded into the deposition chamber. Before deposition, the surfaces of substrates were etched by argon (Ar) plasma treatment. The Ti layer with a thickness of ~ 0.45 μm was firstly deposited on the Si wafers by using a direct current magnetron sputtering (DCMS) system (Chuangshiweina Co. Ltd., MSP-3200T) to sputter a planar round Ti target (purity > 99.95 wt% and diameter of 5.08 cm) with pure Ar (purity > 99.99%). The Ti layer on p-Si wafers can afford a conduction function for photoinduced electrons and serve as an adhesion layer for subsequent growth of the TiO_2 film. The work pressure, DC power and deposition time for Ti layer were fixed at 2 Pa, 400 W and 20 min, respectively. After the deposition of Ti layer, various TiO_2 films were fabricated on all of the five substrates by the DCMS system in the mixed Ar/O_2 (1:1) atmosphere. During the deposition, the work pressure, Ar flow rate and O_2 flow rate were kept at 2 Pa, 20 sccm and 20 sccm, respectively. To tune the dominant facets of anatase TiO_2, the power (or power density) charged on the Ti target was 470 (~23.2) and 200 W (~9.8 W cm^{-2}) corresponding to anatase TiO_2 film with dominant (211) facets (labeled as TP211) and (101) facets (labeled as TP101), respectively. Considering the relationship between deposition rate and target power, more deposition time was spent to obtain the same film thickness when the target power was lower. The deposition time of TP211 and TP101 was set as 270 and 660 min, respectively. Although there was no intentional substrate heating, the substrate temperature increased from around 25 to 170 °C in the deposition process of TP211 and TP101 because of the bombardment of the energetic particles on the substrate surface.

When the p-Si wafers were used as the substrates, the assemble of TiO_2 photoanodes was detailedly described below. A metal Cu belt was used to connect to the Ti layer with silver paint. After drying, the entire back side of Si wafer and the connection of Ti layer and Cu belt were encapsulated in epoxy resin, establishing an exposed light-harvesting area of 0.2-1 cm^2. In addition, calibrated digital images and ImageJ software were used to determine the geometrical area of the exposed surface for all the TiO_2

photoanodes.

Preparation of nanoporous TiO_2 photoanode

The Ti films coated on FTO glass and Si wafers by magnetron sputtering system were electrochemically anodized at 15 V for 30 min and 20 V for 30 min at room temperature. Ti film acted as the working electrode, and Pt foil was used as the counter electrode in the anodization process. The electrolyte solute was ethylene glycol (Sigma-Aldrich) containing 0.3 wt% ammonium fluoride (Sigma-Aldrich), 2 vol% deionized water and 10 vol% polyethylene glycol (Sigma-Aldrich). After anodization, the samples were rinsed in deionized water and ethanol and then annealed at 500 °C for 5 h to form the crystalline and nanoporous TiO_2 photoanodes. At last, the photoanodes were processed in a 0.2 M $TiCl_4$ solution for 60 min at room temperature within tight bottles and then rinsed in ethanol.

Physicochemical characterization

The crystalline structure of the TiO_2 photoanodes was studied using a Bruker diffractometer (DAVINCI) and grazing incidence X-ray diffraction (GIXRD) at a grazing angle of 1° and a scan rate of 2° min^{-1}. Raman measurements of the TiO_2 photoanodes were carried out using a WITEC alpha 300R Confocal Raman microscopy instrument (Oxford Instruments, United Kingdom) with a 532 nm argon-ion laser. Before Raman Characterization, the system was calibrated with the Raman peak of Si at 520 cm^{-1}. The laser powers were set at 2 mW to avoid overheating the photoanodes. Field emission scanning electron microscopy (FESEM) with energy dispersive X-ray spectroscopy (EDS) was employed to investigate the morphology and composition of the surface and cross sections (Magellan 400) of TiO_2 photoanodes. High-resolution transmission electron microscopy (HRTEM, Tecnai G2 F20 S-Twin) was applied to observe the cross-sectional microstructures of TiO_2 photoanodes. X-ray photoelectron spectroscopy (XPS) was used to study the chemical composition and oxidation states of TiO_2 photoanodes. These measurements were performed using a Thermo escalab 250XI spectrometer with a monochromatic Al Kα (1486.6 eV) X-ray source at a pass energy of 29.4 eV. The electron binding energy scale was referenced to the C 1s line of adventitious carbon, set at 284.8 eV. Inductively coupled plasma optical emission spectrometry (ICP-OES) was carried out on the Agilent 5110 (America) to quantify the Ti ions in the electrolyte after reactions. UV-visible-near-IR spectrophotometry (Hitachi, UH-4150) was applied to monitor the optical properties of the TiO_2 photoanodes on the BK7 glass. The optical energy band gap of the TiO_2 photoanodes was estimated using the typical relations with the transmittance (T) spectra:

$$\alpha = -\frac{\ln(T)}{h_{\mathrm{f}}} \tag{1}$$

$$\alpha h\nu = B(h\nu - E_{\mathrm{g}})^{\mathrm{m}} \tag{2}$$

where h_{f}, α, $h\nu$, B and E_{g} denote the thickness of TiO_2 film, absorption coefficient, photon energy, band tailing parameter and optical band gap, respectively. The value m for the TiO_2 film is 2 corresponding to the indirect allowed transition. The light harvesting efficiency (η_{lhe}) is calculated from the absorbance data (η_{a}) via the following equation.

$$\eta_{\mathrm{lhe}} = \left(1 - 10^{-\eta_{\mathrm{a}}}\right) \times 100\% \tag{3}$$

The corresponding adsorption spectra of the samples were derived from transmittance spectra through the relation,

Absorption = 100 – transmittance – reflectance (4)

assuming zero reflectance for the TiO_2 films. Photoluminescence (PL) spectra were acquired at room temperature on a fluorescence spectrophotometer (Fls-980, Edinburgh) with an excitation wavelength of 380 nm. Time-resolved PL (TRPL) decay spectra were carried out via a fluorescence lifetime spectrometer. The PL lifetime of the TiO_2 photoanodes was fitted with the experimental decay transient data using a bi-exponential decay model.

Wettability determination

The hydrophilicity of the TiO_2 photoanodes was determined by measuring the contact angle (CA) of an electrolyte droplet (1 M KOH) on the surface. The method of digital video image was used to process the sessile droplets by a contact angle apparatus (Chengde Dingsheng Testing Machine Co. Ltd., JY-82A) under ambient conditions at room temperature. A CCD camera with a space resolution of 1280 × 1024 and a color resolution of 256 gray levels was applied in the capture of droplet images. A droplet (~5 μL) of 1 M KOH was injected onto the surface using a 1 mL micro-injector. The CA values for each TiO_2 photoanode at 5 min were obtained and confirmed repeatedly.

Stress measurements

The isotropic biaxial stress of the TiO_2 films was acquired from the radius of curvature technique which compared the curvatures of the Si wafers before and after depositing TiO_2 films. The stress was calculated via Stoney's equation in the tester:

$$\sigma = -\frac{E_s h_s^2}{6(1-\upsilon_s)h_f}\left(\frac{1}{R_{af}} - \frac{1}{R_{be}}\right) \quad (5)$$

where E_s, υ_s, h_s and R_{be} are the elastic modulus, Poisson's ratio, thickness and spherical radius curvature of the Si wafer, respectively, and R_{af} is the spherical radius curvature of the TiO_2 film coated on the Si wafer. The E_s, υ_s and h_s of Si wafer serve as 131 GPa, 0.2782 and 500 μm, respectively. The film thickness of TP211 and TP101 was ~1.4 μm tested by FESEM and HRTEM. Before and after the deposition of TiO_2 film, the radius of curvature of each Si wafer was monitored by Micro XAM-3D Surface Profile. For each Si wafer, five measurements were carried out.

Ferromagnetic evaluation

Magnetization (M) versus applied magnetic field (H) at room temperature was monitored in a Quantum Design superconducting quantum interference device (SQUID, Quantum DesignXL7) magnetometer. The applied magnetic fields were vertical and parallel to the surface of the TiO_2 photoanodes, respectively. The magnetization data of the TiO_2 photoanodes have been corrected to avoid the interference of the diamagnetism of Si wafer. Typical net magnetic moments for the TiO_2 photoanodes used in this work were of the order of 10^{-4}-10^{-6} emu absolute, which are approximately two-four orders of magnitude higher than the base sensitivity of the SQUID magnetometer.

Electrical measurements

Photo-assisted Kelvin probe force microscopy (KPFM) measurements for TiO_2 photoanodes were measured using a Bruker multimode microscope controlled by an NTEGRA III unit coupled to a Nanonis control unit (SPECS Zürich) under ambient conditions. The KPFM electrical excitation was made at a frequency $\omega/2\pi$ of 80 Hz, with a VAC amplitude of 500 mV. The TiO_2 photoanodes were irradiated by the light from the top. In the setup, conductive Nanosensors tips were used at a resonant frequency of about 75 kHz. In this work, no calibration of the tip work function was necessary since the obtained surface potential difference (V_{spd}) only varied with the photovoltaic blends of the TiO_2 photoanodes. The changes of V_{spd} were relative but quantitative with regard to variations in the surface potentials of the studied TiO_2 interfaces.

Current versus Voltage (*I-V*) curves were performed using a GPS150 probe station equipped with an HW-1616 constant temperature controller and a Keithley 2400 digital source meter. The Xe lamp with an AM 1.5G filter was used for illumination, and calibrated to AM 1.5 intensity (100 mW·cm-2) through a light power meter (PerfectLight Co. Ltd., PL-MW 200). Before the measurement of the light current, each TiO_2 photoanode was cut into 5 × 5 mm2 and then glued onto one quartz glass with conductive silver paint (Leitsilber 200). Part of the dried silver paint on the glass, which was exposed to air, functions as one electrode, while another electrode is produced by dotted the silver paint on the surface of each TiO_2 photoanode. Tungsten probes were used to contact a front and back collector for dry measurements. To obtain the light current, the voltage range was all set at -2.0 V ~2.0 V with or without irradiation.

Mechanical properties

Scratch tests were used to measure the adhesion force of the TiO_2 photoanodes on FTO glass with a loading rate of 25 N min^{-1} by a scratch tester (Kaihua MFT-4000, China). The critical load and the adhesion failure were identified when the curve of friction versus (vs.) load had a sudden shift. The morphology of the scratch scar after testing was observed and analyzed by a metallographic microscope. The hardness and elastic modulus were performed by using a nanoindenter (Bruker Hysitron TI980) with a Berkovich diamond tip. The mean value of the hardness and elastic modulus of the TiO_2 film was obtained from the loading-unloading curves over 3 times. The indentation depth was about 10% of the film thickness to reduce the influence of substrate materials. To testify its flexibility, the metallographic analysis of TP211 before and after bending was carried out by the metallographic microscope.

The tribological behaviours of the TiO_2 photoanodes were evaluated by a tribometer device (MFT-EC 4000, China) at room temperature of about 20±5 °C and humidity of 70±5%. In the sliding process, the AISI52100 steel balls were used as the counterparts with a diameter of 6 mm. The tests were done at a sliding speed of 600 rpm and a sliding stroke of 4 mm. The normal load was 1.0 N, corresponding to a theoretical initial Hertzian contact pressure of ~0.5 GPa. After the tribological tests, the 3D surface profiler (MixroXAM 800, America) was used to observe the depth and width of the wear track and calculate the wear volume. Then the wear rate (*W*) was figured out with the following equation:

$$W = \frac{V}{ND} \tag{6}$$

where *V*, *N* and *D* are denoted as the wear volume, normal load and sliding distance, respectively.

Photoelectrochemical measurements

A three-electrode cell containing the TiO_2 photoanode, the counter electrode of Pt mesh and the Ag/AgCl reference electrode, was used in PEC measurements using a PEC 1000 system (PerfectLight Co. Ltd.) with solar light (AM 1.5G, 100 mW·cm^{-2}) of a solar simulator (optical fiber source, FX300). The solar simulator intensity was calibrated using a reference silicon solar cell and a readout meter (PerfectLight Co. Ltd., PL-MW 200) before each measurement. Aqueous KOH (1.0 M) served as the electrolyte unless noted otherwise. Line-sweep voltammetry (*J*-potential curve) measurements were collected using a CHI 750E electrochemical workstation with or without illumination. The voltage was linearly swept at a scan rate of 5 mV·s^{-1} during *J*-potential measurements. Readings for Ag/AgCl were converted to RHE as follows.

$$E(\mathrm{RHE}) = E(\mathrm{Ag/AgCl}) + 0.197 + 0.059 \times \mathrm{pH} \tag{7}$$

The chronoamperometry measurements (namely *J-t* curves) of TiO_2 photoanodes were carried out

over 1100 h in 22-mL electrolytes (1 M KOH) at 0.6 V vs. RHE to confirm their stability. The photoelectrochemically active surface of TiO_2 photoanodes was carried out by cyclic voltammetry (CV) with scan rates of 20, 40, 60, 80 and 100 mV s^{-1}. The double-layer capacitance (C_{dl}) was estimated by plotting the ΔJ at different potentials against the scan rates. Electrochemical impedance spectroscopy (EIS) measurements of TiO_2 photoanodes were performed by an Autolab electrochemical workstation (Autolab PGSTAT302N, MetrohmAutolab BV, Netherlands) over a frequency range from 0.1 MHz to 0.1 Hz in the dark. The EIS measurements of TP211 and TP101 were measured at 0.21 and 0.06 V vs. RHE in 1.0 M KOH, respectively. The Mott-Schottky plots were acquired at a frequency range of 1.0-3.0 KHz in 1.0 KOH solution by a CHI 750E electrochemical workstation. The Mott-Schottky equation is shown below:

$$\frac{1}{C^2} = \frac{2}{q\varepsilon_s\varepsilon_0 A^2 N_D}(V - V_{fb} - \frac{kT}{q}) \quad (8)$$

C is capacitance, q the charge of an electron (1.60 ×10^{-19} C), ε_0 the vacuum permittivity (8.85 ×10^{-14} F cm^{-1}), ε_s the permittivity of TiO_2, A the area of the photoanode, N_D the donor density, V the applied bias, V_{fb} the flat band voltage, k Boltzmann's constant (1.38 ×10^{-23} J K^{-1}), and T the temperature (25 °C). The x-intercept of Mott-Schottky plots was reached at the bias that needs to be applied to cause the bands to become flat. The x-intercept plus kT/q (~0.025 V) equals the flat band voltage. Also, the slope of the plots can be used to calculate the donor density of the photoelectrode. The donor density (N_D) can be calculated using the equation:

$$N_D = \frac{2}{e\varepsilon\varepsilon_0}\left[\frac{d\left(1/C^2\right)}{dV}\right]^{-1} \quad (9)$$

where ε and $\left[\frac{d\left(1/C^2\right)}{dV}\right]$ are the dielectric constant of TiO_2 and the slope of the sharp increase from 0.2 to 0.4 V vs. RHE.

FTO glass with an area of 10 × 10 cm^2 was selected as the substrate. During the deposition, the blank area of ~2 × 3 cm^2 on the surface of the FTO glass was kept for installing the Si-based photocathode, and the rest area was firstly deposited with TP211. Subsequently, the titanium-covered surface was deposited with TiO_2. The etched p-Si wafers, that were obtained by a 2% potassium hydroxide aqueous solution in an 80 °C water bath for 1 h, were regarded as excellent light absorbers. The amorphous TiO_2 layer and Fe cocatalysts were orderly deposited on the etched p-Si wafer to form an efficient Si-based photocathode for NO_3^- reduction reaction. Then, the prepared Si-based photocathode was pasted with silver glue on the blank area of FTO glass and encapsulated in epoxy resin. The electrolytes were 1 M KOH and 50 mM KNO_3 aqueous solutions. The free-wired device of TP211-Si-based photocathode with the electrolytes was put outside on a sunny day at noon in Changsha City, Hunan Province, China to

carry out the oxygen evolution reaction and NO_3^--to-NH_3 synthesis.

Supplementary figures

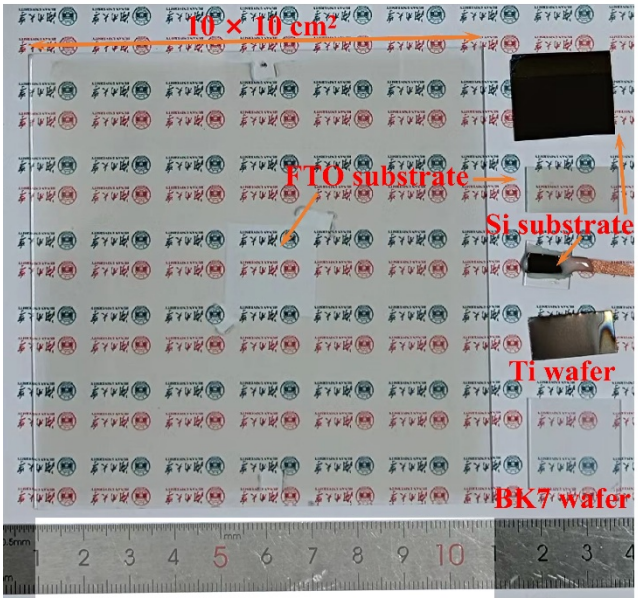

Figure S1. Photograph of TP211 on various substrates with different scales (e.g., 10 × 10 cm^2 area).

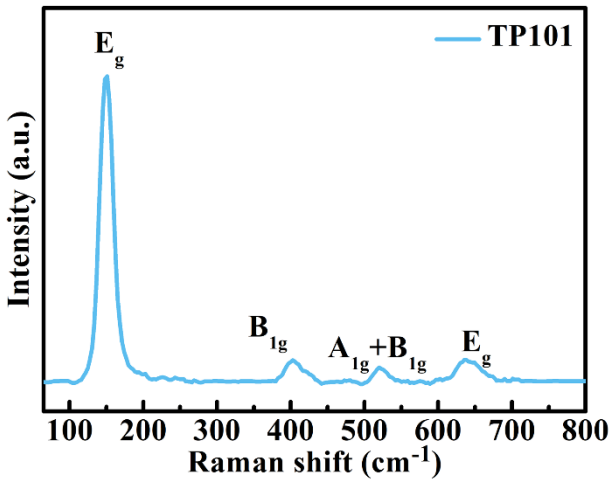

Figure S2. Raman spectrum of TP101.

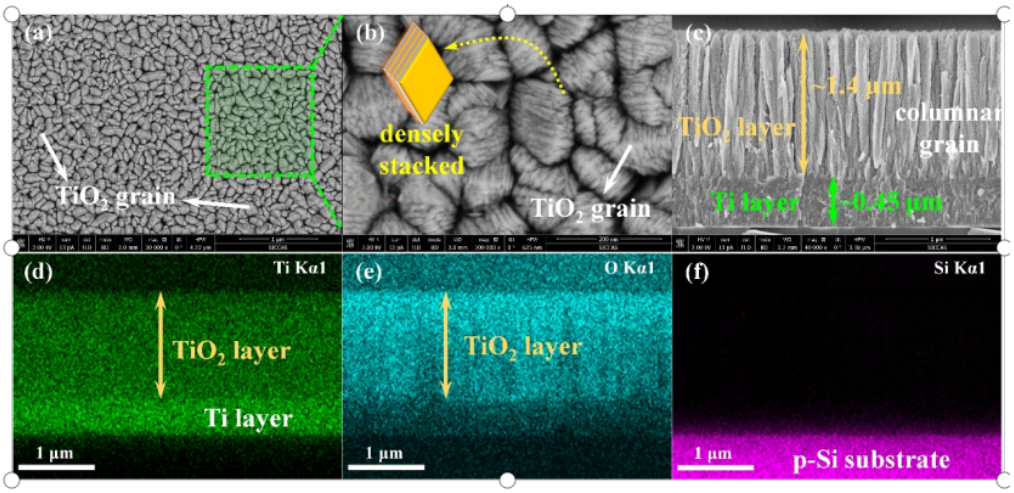

Figure S3. FESEM images of TP211. (a) Top-view image with low magnification. (b) High-magnification image of the specified area in (a). The inset is the schematic diagram of a TiO_2 grain with dominant (211) facets. (c) Cross-sectional image. (d-f) Corresponding EDS mapping from cross-sectional view: (d) Ti Kα1; (e) O Kα1; (f) Si Kα1.

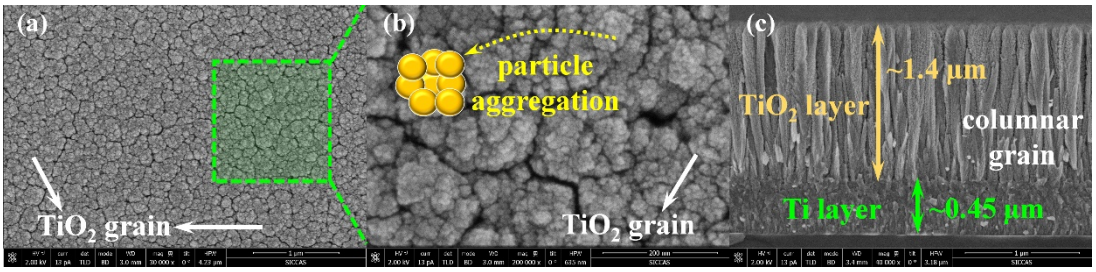

Figure S4. FESEM images of TP101. (a) Top-view image with low magnification. (b) High-magnification image of the specified area in (a). The inset is the schematic diagram of a TiO_2 grain with dominant (101) facets. (c) Cross-sectional image.

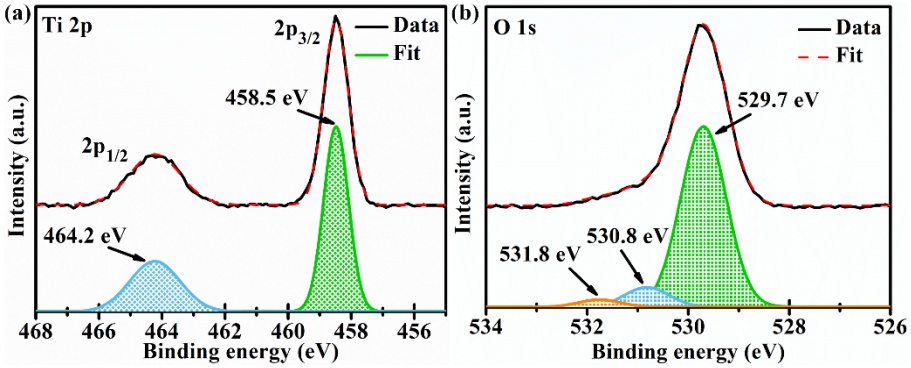

Figure S5. XPS spectra of TP211: (a) Ti 2p; (b) O 1s.

The dominant peak of Ti $2p_{3/2}$ for TP211 was centered at 458.5 eV (see Figure S4a) ascribed to Ti^{4+}, which is in line with the O-Ti bonds of 529.7 eV in the O 1s spectrum. No peaks ascribed to Ti^{3+} were observed on the surface of TP211 via XPS measurements.

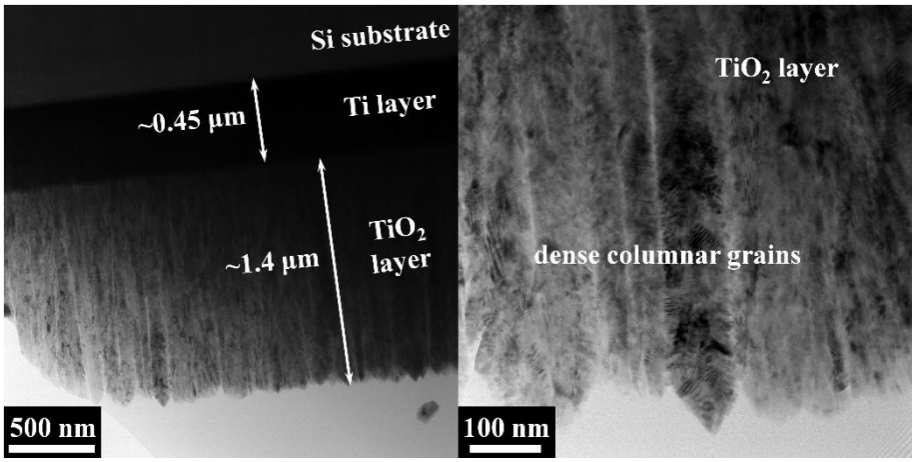

Figure S6. HRTEM images of TP211 with low (left) and high (right) magnification.

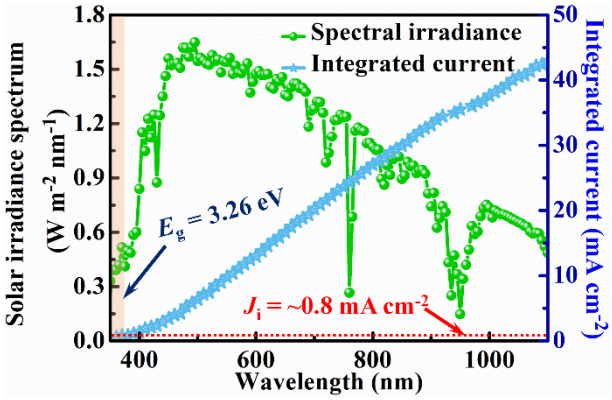

Figure S7. Irradiance and integrated current of AM 1.5G solar spectrum. Photocurrent density (J_i) at 100% internal quantum efficiency and 100% light harvesting efficiency can be estimated by the integrated current at the photoanodes across the wavelength range.

When the band gap is 3.26 eV corresponding to the maximal adsorption wavelength of ~380 nm, the J_i value of TP211 is calculated as ~0.8 mA cm^{-2}.

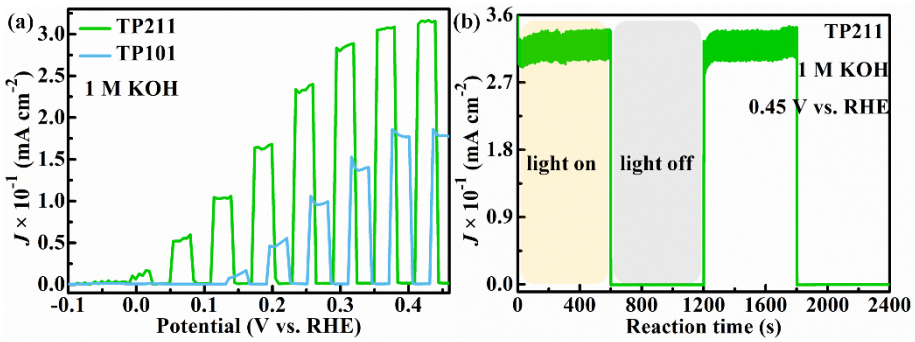

Figure S8. (a) The comparison of PEC water oxidation performance for TP211 and TP101 by chopped *J*-potential curves measured in 1 M KOH under AM1.5 G simulated sunlight (100 mW cm^{-2}). (b) Chopped *J*-time curves of TP211 at the fixed potential of 0.45 V vs. RHE in 1 M KOH.

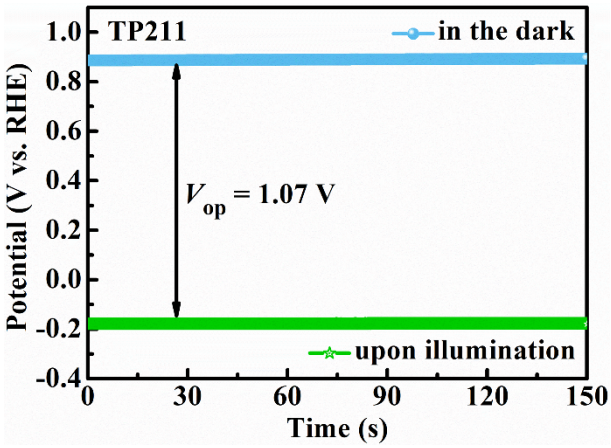

Figure S9. Open-circuit potential (OCP) of TP211 in 1 M KOH in the dark and upon illumination.

The negative shift in OCP upon illumination indicates that TP211 possesses n-type conductivity. The difference of OCP for TP211 in the dark and upon illumination shows a high photovoltage (V_{ph}) of 1.07 V.

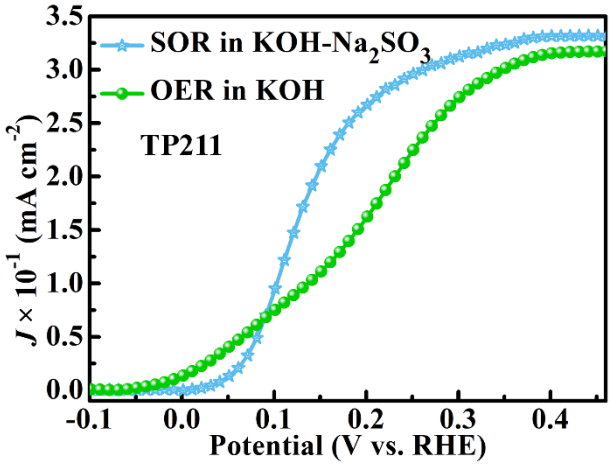

Figure S10. The comparison of PEC water oxidation and sulfite oxidation for TP211 by *J*-potential curves under AM1.5 G simulated sunlight (100 mW cm^{-2}). The sulfite oxidation was measured in 1 M KOH electrolytes with 0.05 M Na_2SO_3.

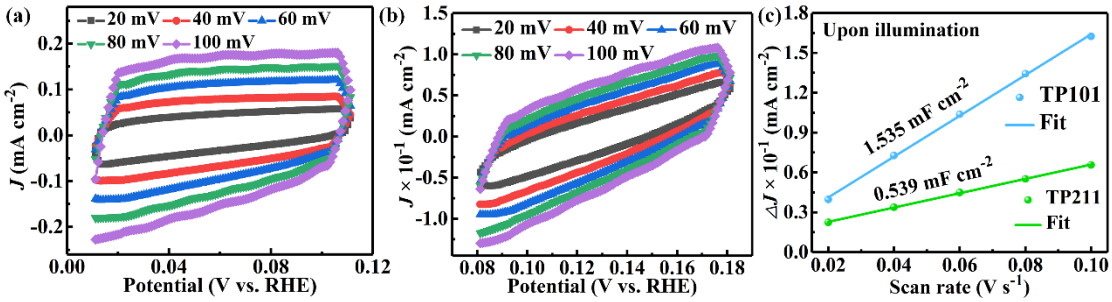

Figure S11. Photoelectrochemical surface areas of TiO_2 photoanodes measured under AM1.5 G simulated sunlight (100 mW cm^{-2}). (a) Photoelectrochemical cyclic voltammetry curves of TP101 with scan rates at 20, 40, 60, 80 and 100 mV s^{-1}. (b) Photoelectrochemical cyclic voltammetry curves of TP211 with scan rates at 20, 40, 60, 80 and 100 mV s^{-1}. (c) Photoelectrochemical double-layer capacitance (C_{dl})

values of TP101 and TP211 determined by the capacitive current at certain applied potential.

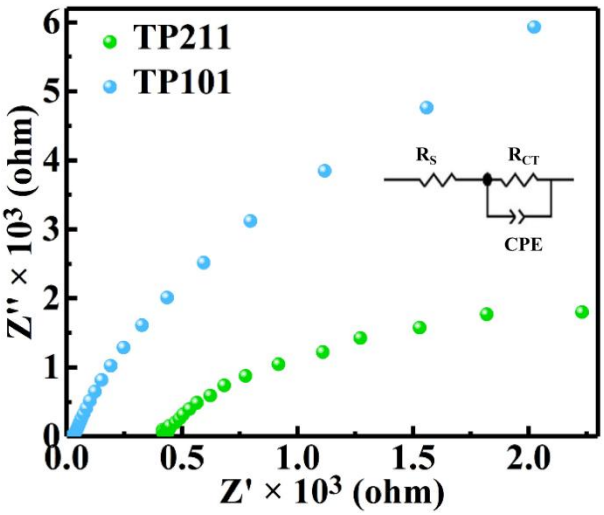

Figure S12. EIS Nyquist plots of TP101 and TP211 at 0.21 V vs. RHE in the dark.

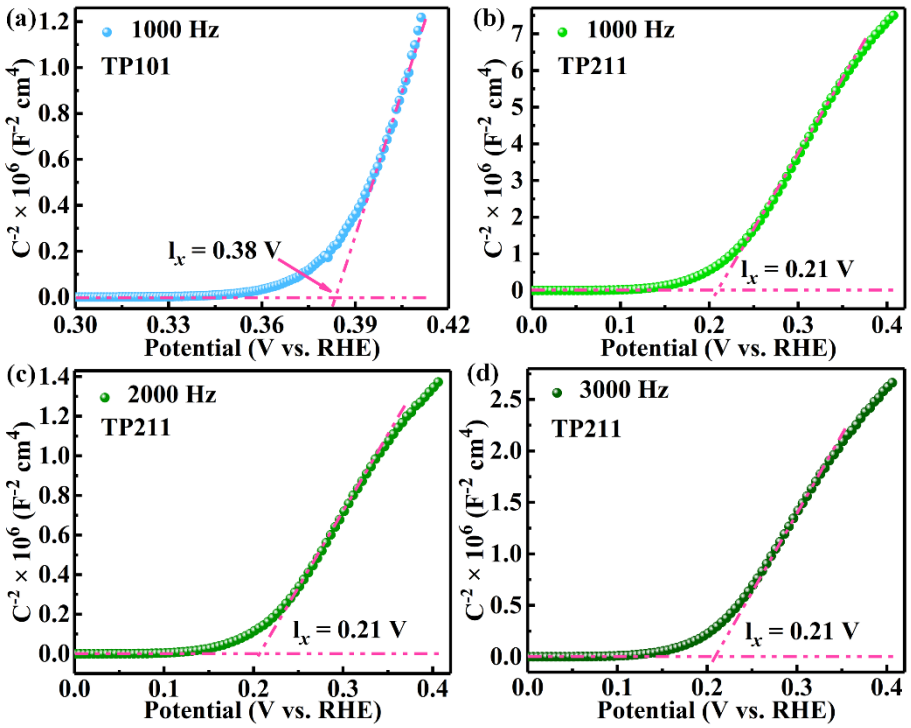

Figure S13. Mott-Schottky plots of TiO_2 photoanodes collected with different frequencies upon illumination by using a CHI 750E electrochemical workstation. (a) TP101 by a frequency of 1 KHz. (b) TP211 by a frequency of 1 KHz. (c) TP211 by a frequency of 2 KHz. (d) TP211 by a frequency of 3 KHz.

Mott-Schottky (M-S) plots of TP101 and TP211 were measured and shown in Figure S13. Additionally, the donor density (N_d) or charge carrier density is inversely proportional to the slope of the sharp increase in M-S plots, as shown in Equation S9. Due to the larger slope, TP211 shows a smaller N_d than TP101. Finally, TP211 and TP101 are the classic n-type semiconductors with a positive slope in the M-S plots.

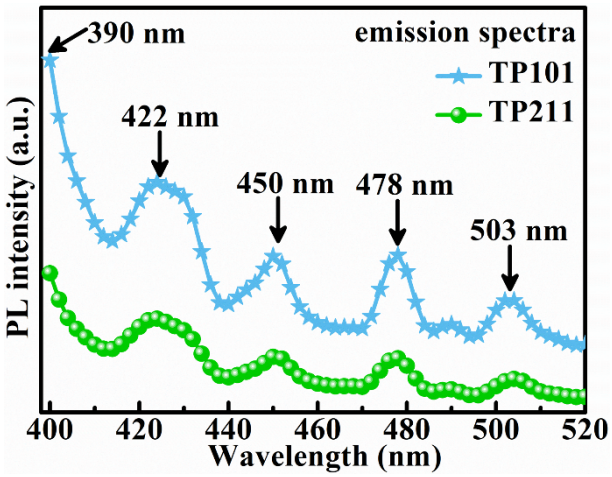

Figure S14. Room temperature PL spectra of TP211 (green) and TP101 (blue) with an excitation wavelength of 380 nm. For TiO_2, five main emission peaks were located at about 390, 422, 450, 478 and 503 nm labeled by dark arrows, which are equivalent to 3.17, 2.93, 2.75, 2.59 and 2.46 eV, respectively. The relatively strong PL peak at about 390 nm is usually ascribed to the emission of bandgap transition with the energy of light approximately equal to the bandgap energy of anatase (211) (380 nm). The PL bands from 2.93 eV to 2.46 eV are ascribed to the surface-state trapped exciton emission for TiO_2 grains, including single, two and three phonon-one photon coupling course with the $E_g(v1)$ and $B_{1g}(v2)$ phonon attendance and assistance. In comparison to TP101, a considerable fluorescence quenching was observed in TP211. The quenching of fluorescence indicates a faster separation and transfer of photoinduced charge carriers in TP211.

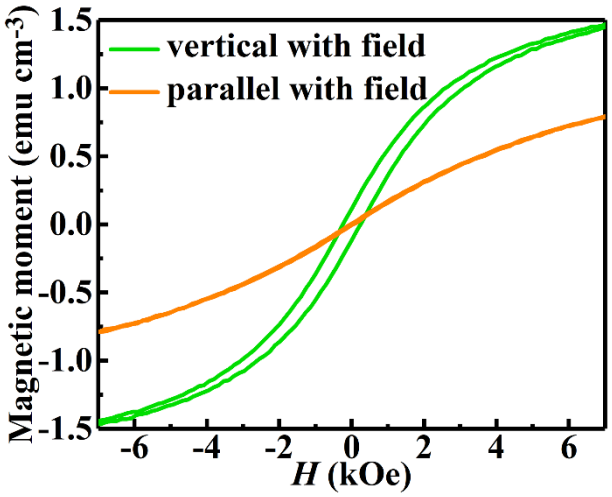

Figure S15. Room temperature hysteresis curves of TP211 with applied magnetic field vertical (green) and parallel (orange) with the surface.

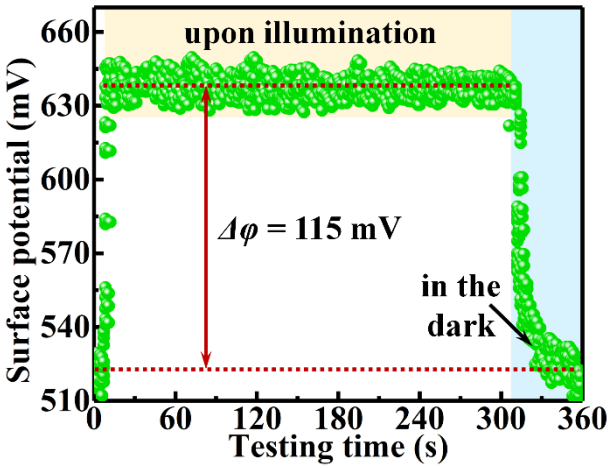

Figure S16. Surface potential-testing time curves of TP211 obtained from KPFM upon illumination with 380 nm and in the dark.

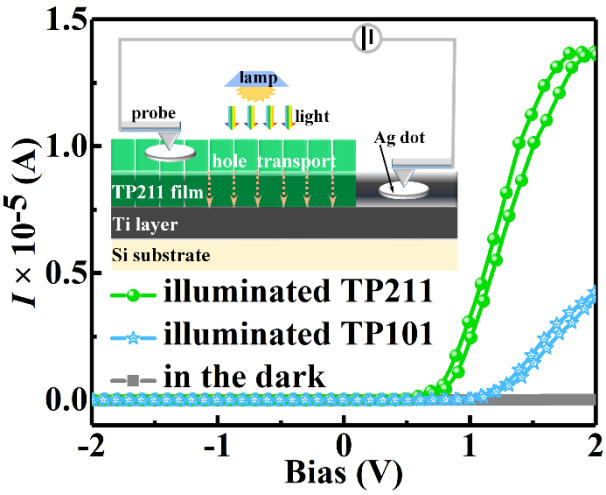

Figure S17. Current-applied bias curves of TP211 and TP101 measured in a probe station (no electrolyte present) upon illumination and in the dark. The measurement was carried out at the Ag contact through the TiO_2 film, as shown in the inset of Figure S18.

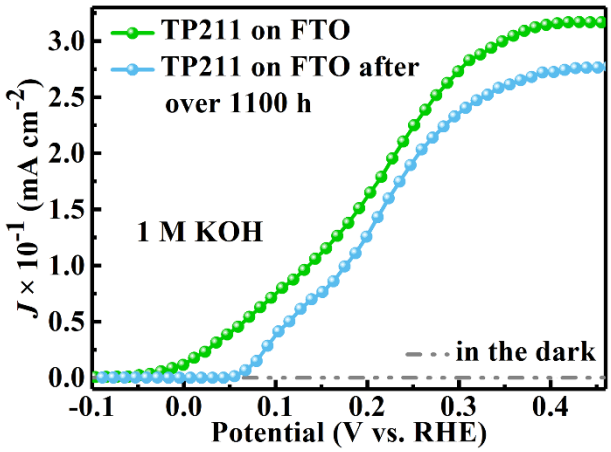

Figure S18. *J*-potential plots of TP211 on FTO glass wafer measured in 1 M KOH under 1 sun illumination before and after over 1100-h PEC water splitting.

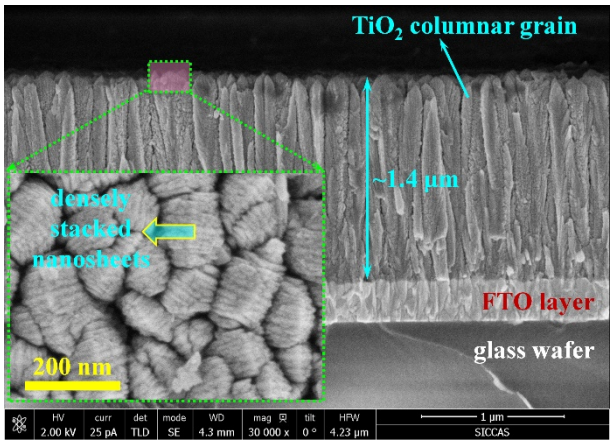

Figure S19. Cross-sectional FESEM image of TP211 on FTO glass wafer after over 1100-h PEC water splitting. The inset is the corresponding top-view FESEM image of the reacted photoanode.

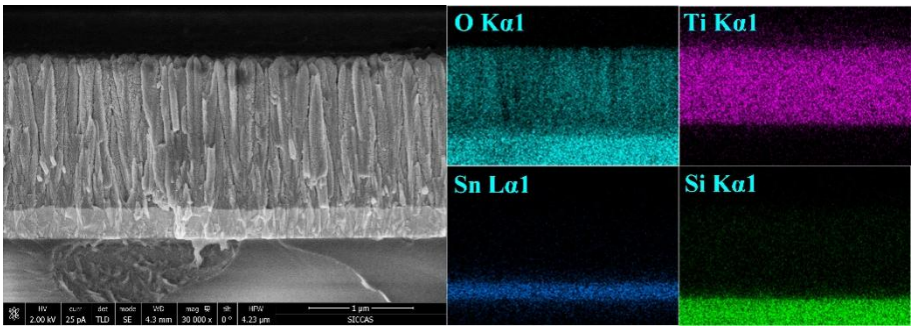

Figure S20. FESEM images of TP211 on FTO glass wafer after over 1100-h PEC water splitting, including cross-sectional image and corresponding EDS mapping of O Kα1, Ti Kα1, Sn Lα1 and Si Kα1.

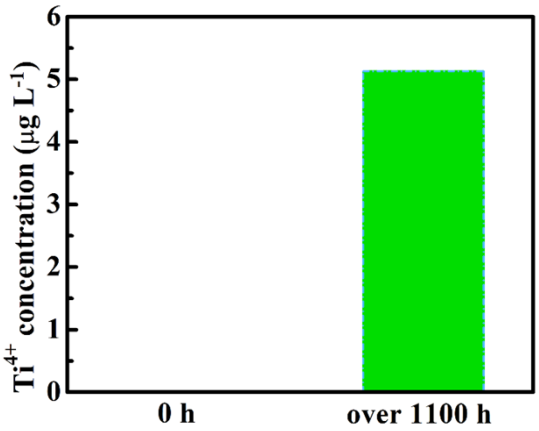

Figure S21. Concentration of Ti^{4+} ions in the 1 M KOH electrolytes before and after over 1100-h PEC water splitting.

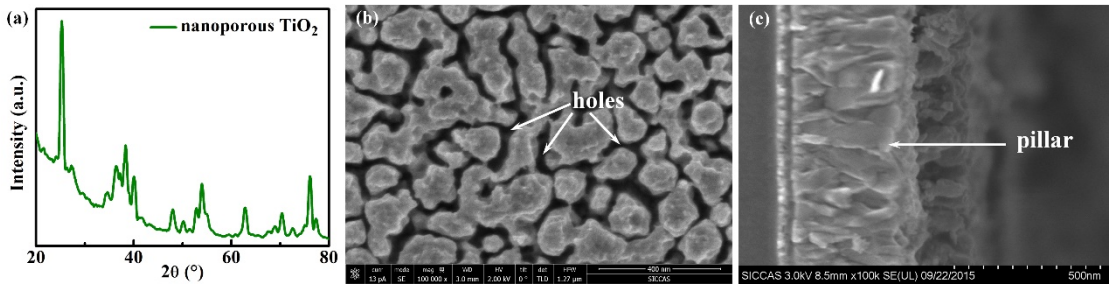

Figure S22. Characterization of nanoporous TiO_2 photoanode. (a) XRD pattern. (b) Top-view FESEM image. (c) Cross-sectional FESEM image.

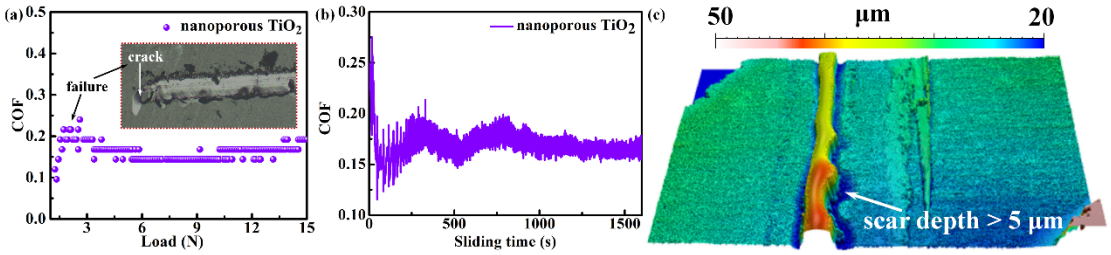

Figure S23. (a) Scratch test curves of nanoporous TiO_2 photoanode with COF signal. The inset is the micrograph of the scratch track at the initial and terminal steps. (b) COF curve of nanoporous TiO_2 photoanode against AISI52100 steel ball. (c) 3D image of wear scar on the surface of nanoporous TiO_2 photoanode after tribological measurement.

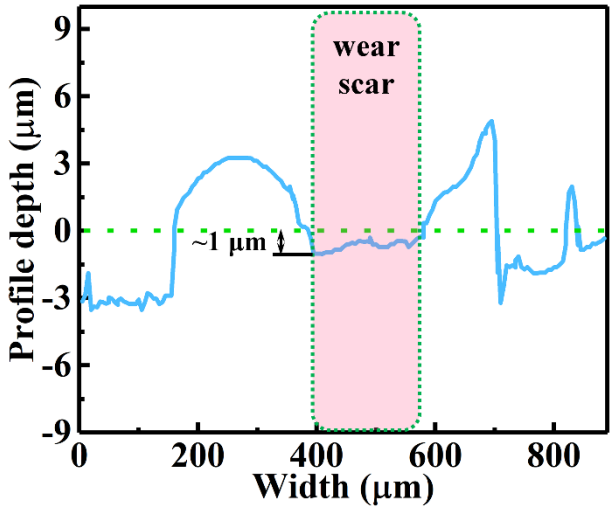

Figure S24. The cross-sectional profile of wear scar on the surface of TP211 after tribological measurement.

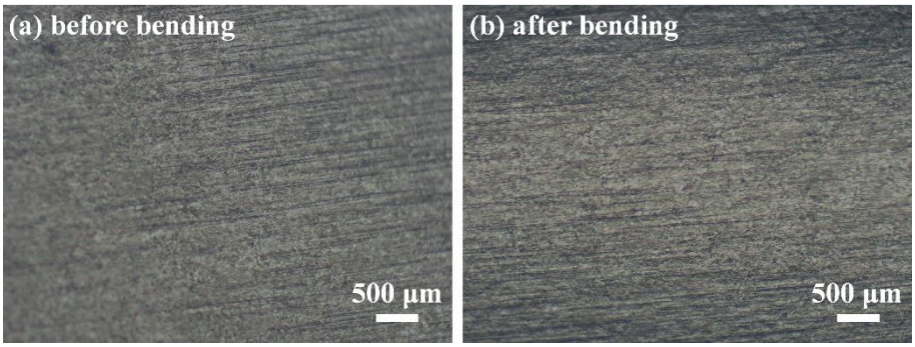

Figure S25. Metallographic analysis of TP211 on Ti foil before (a) and after (b) bending.

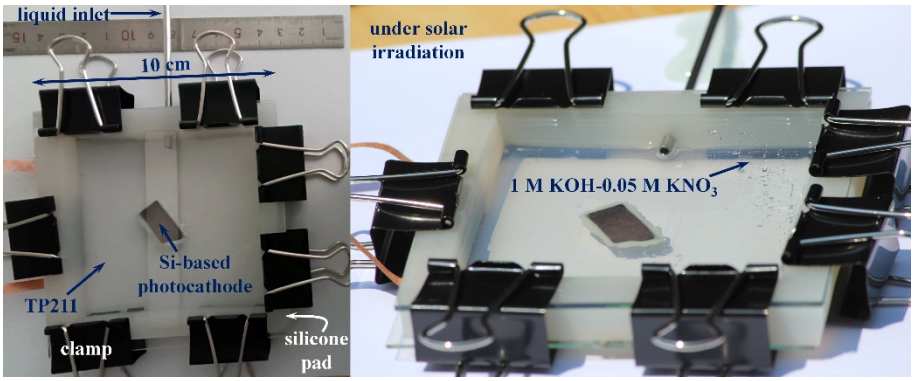

Figure S26. (a) The configuration of large-scale TP211 photoanode/Si-based photocathode device, mainly including ~60.6-cm^{-2} TP211 photoanode and ~1.8-cm^{-2} Si-based photocathode (Fe/TiO_2/Fe/Si multilayer structure). (b) PEC OER and NO_3^- reduction reaction of the device in 1 M KOH with 0.05 M KNO_3 directly carried out under solar irradiance in the ambient.

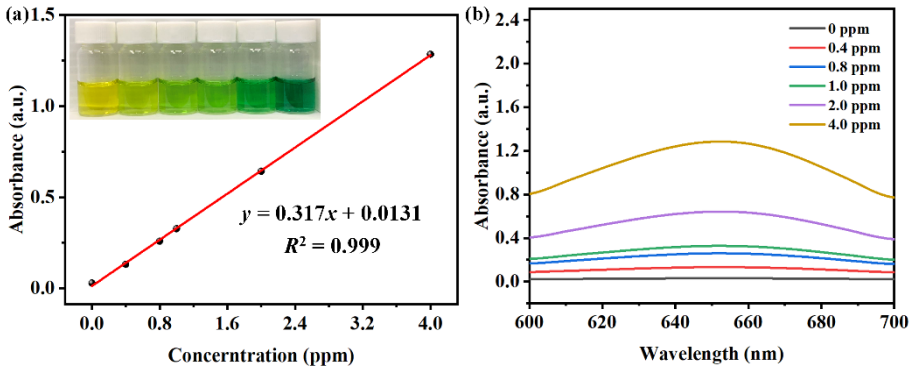

Figure S27. Absolute calibration of the indophenol blue method using NH_4^+-containing solutions of known concentration as standards. (a) Calibration curve used for the determination of NH_3 by NH_4^+ ion concentration. The absorbance at ~650 nm was measured by UV-visible spectrophotometry. The fitting curve shows an excellent linear relationship between absorbance and NH_4^+ ion concentration (y = 0.317x + 0.0131, R^2 = 0.999) in three independent calibration curves. The inset in (a) shows the chromogenic reaction of the indophenol indicator with NH_4^+ ions. (b) UV-visible spectroscopy curves of indophenol assays with NH_4^+ ions after incubation for 2 hours.|

Table S1. Calculated surface energies (E) and surface densities of fivefold-coordinated Ti_5, fourfold-coordinated Ti_4, and twofold-coordinated oxygen O_2 atoms [n (Ti_5), n (Ti_4), and n (O_2)]. N_{at} is the total number of atoms in the slab.

Facet	N_{at}	E (J/m^2)	n (Ti_5) (10^{-2} Å^{-2})	n (Ti_4) (10^{-2} Å^{-2})	n (O_2) (10^{-2} Å^{-2})
(101)[1]	24	0.52	5.1		5.1
(001)[1]	18	1.08	6.9		6.9
(211)[1]	54	0.97	2.4	2.4	7.2
(103)[2]	48	0.99		3.5	
(110)[2]	42	1.15		3.8	

Table S2. Summary of important performance metrics reported in recent publications of TiO_2-based photoanodes. The saturated photocurrent density and corresponding applied bias are simplified as J_{sa} and V_{ap}, respectively.

Photoanode materials	Thickness (nm)	Surface area	J_{sa} (mA cm^{-2})	Corresponding V_{ap} at J_{sa} (V)	Light source	Ref.
TiO_2 film with dominant (211) facets	1400	Very low	**0.32**	**0.45**	AM 1.5G	**This work**
TiO_2 film	65	Very low	0.04	1.8	UV light	(1)[3]
TiO_2 film	50	Very low	0.025	1.23	UV light	(2)[4]
TiO_2 film	<100	Low	5.3×10^{-4}	1.23	AM 1.5G	(3)[5]
TiO_2 film	<100	Low	0.054	0.5	UV light	(4)[6]
N-doped TiO_2 film	>100	Low	0.077	1.2	AM 1.5G	(5)[7]
TiO_2 film	>1000	Medium	0.011	1.8	UV light	(6)[8]
TiO_2 film	--	Medium	0.042	1.23	UV light	(7)[9]
TiO_2 film	>1000	Medium	0.08	1.23	UV light	(8)[10]
Sn-doped TiO_2 film	>1000	High	0.14	1.5	AM 1.5G	(9)[11]
PANI/GO/TiO2	>100	High	0.12	1.23	AM 1.5G	(10)[12]
Ag/porous TiO_2 film	>1000	High	0.05	1.0	AM 1.5G	(11)[13]
Nanoporous TiO_2 film	--	Very high	1.5×10^{-4}	1.0	UV light	(12)[14]
Nanoporous TiO_2 film	4000	Very high	0.093	1.23	UV light	(13)[15]
Graphene-porous TiO_2	>1000	Very high	0.032	1.23	AM 1.5G	(14)[16]
C@TiO_2 porous film	9000	Very high	0.35	1.6	AM 1.5G	(15)[17]

$TiO_2/BiVO_4$ nanorods	1500	Very high	0.04	1.23	AM 1.5G	(16)[18]
TiO_2 nanorods	4500	Very high	0.23	1.8	AM 1.5G	(17)[19]
TiO_2 nanorods	1500	Very high	0.05	--	AM 1.5G	(18)[20]
TiO_2 nanotubes	>1000	Very high	0.07	1.2	AM 1.5G	(19)[21]
N-doped TiO_2 nanowires	>1000	Very high	0.2	1.5	AM 1.5G	(20)[20]
FeS_2/TiO_2 nanotubes	>1000	Very high	0.043	1.0	Visible light	(21)[22]
Mo-doped TiO_2 nanotubes	>1000	Very high	0.23	1.23	UV light	(22)[23]
TiO_2 film	1200	Very low	0.14	0.6	AM 1.5G	(23)[24]

Reference:

1. Xu, J. ; Xu, L.; Li, Z.; Wang, J.; Lin, Z.; Liu, K.; Cao, Y., *Ab Initio* Study of Water Adsorption and Reactivity on the (211) Surface of Anatase TiO_2. *Physical Review Applied* **2016**, 5, 064001.
2. Lazzeri, M.; Vittadini, A.; Selloni, A., Structure and energetics of stoichiometric TiO_2 anatase surfaces. *Physical Review B* **2001**, 63, 155409.
3. Krysa, J.; Zlamal, M.; Kment, S.; Brunclikova, M.; Hubicka, Z., TiO_2 and Fe_2O_3 Films for Photoelectrochemical Water Splitting. *Molecules* **2015,** *20* (1), 1046-1058.
4. Cheng, H.-E.; Chen, C.-C., Morphological and Photoelectrochemical Properties of ALD TiO_2 Films. *Journal of The Electrochemical Society* **2008,** *155* (9), D604.
5. Zhan, X.; Peng, Z.; Huang, H.; Zhang, H.; Liu, Z.; Ou, X.; Yang, F.; Liu, Z., Photoelectrochemical performance enhancement of low-energy Ar+ irradiation modified TiO_2. *Applied Surface Science* **2021,** *541*, 148527.
6. Li, X.; Gao, C.; Duan, H.; Lu, B.; Pan, X.; Xie, E., Nanocrystalline TiO_2 film based photoelectrochemical cell as self-powered UV-photodetector. *Nano Energy* **2012,** *1* (4), 640-645.
7. Garlisi, C.; Lai, C.-Y.; George, L.; Chiesa, M.; Palmisano, G., Relating Photoelectrochemistry and Wettability of Sputtered Cu- and N-Doped TiO_2 Thin Films via an Integrated Approach. *The Journal of Physical Chemistry C* **2018,** *122* (23), 12369-12376.
8. Gong, J.; Yang, C.; Pu, W.; Zhang, J., Liquid phase deposition of tungsten doped TiO_2 films for visible light photoelectrocatalytic degradation of dodecyl-benzenesulfonate. *Chemical Engineering Journal* **2011,** *167* (1), 190-197.
9. Jiang, D.; Zhao, H.; Zhang, S.; John, R.; Will, G. D., Photoelectrochemical measurement of phthalic acid adsorption on porous TiO_2 film electrodes. *Journal of Photochemistry and Photobiology A: Chemistry* **2003,** *156* (1), 201-206.
10. Yoko, T.; Hattori, T.; Kozuka, H.; Zhao, G.-L.; Lin, H., Preparation and Photoelectrochemical Properties of TiO_2 Films Consisting of Monodispersed Particles by Sol-Gel Method. *Molecular Crystals and Liquid Crystals Science and Technology. Section A. Molecular Crystals and Liquid Crystals* **1999,** *337* (1), 221-224.
11. Sohail, M.; Baig, N.; Sher, M.; Jamil, R.; Altaf, M.; Akhtar, S.; Sharif, M., A Novel Tin-Doped Titanium Oxide Nanocomposite for Efficient Photo-Anodic Water Splitting. *ACS Omega* **2020,** *5* (12), 6405-6413.

12. Yuan, X.; Xu, Y.; Meng, H.; Han, Y.; Wu, J.; Xu, J.; Zhang, X., Fabrication of ternary polyaniline-graphene oxide-TiO_2 hybrid films with enhanced activity for photoelectrocatalytic hydrogen production. *Separation and Purification Technology* **2018,** *193*, 358-367.

13. Guitoume, D.; Achour, S.; Sobti, N.; Boudissa, M.; Souami, N.; Messaoudi, Y., Structural, optical and photoelectrochemical properties of TiO_2 films decorated with plasmonic silver nanoparticles. *Optik* **2018,** *154*, 182-191.

14. Wang, G.-L.; Xu, J.-J.; Chen, H.-Y., Dopamine sensitized nanoporous TiO_2 film on electrodes: Photoelectrochemical sensing of NADH under visible irradiation. *Biosensors and Bioelectronics* **2009,** *24* (8), 2494-2498.

15. Park, J.-J.; Kim, D.-Y.; Lee, J.-G.; Cha, Y.-H.; Swihart, M. T.; Yoon, S. S., Supersonic aerosol-deposited TiO_2 photoelectrodes for photoelectrochemical solar water splitting. *RSC Advances* **2014,** *4* (17), 8661-8670.

16. Nguyen Van, C.; Thanh Hai, N.; Olejnicek, J.; Ksirova, P.; Kohout, M.; Dvorakova, M.; Van Hao, P.; Ngoc Hong, P.; Cuong Tran, M.; Hoang Tung, D.; Van Thanh, D., Preparation and photoelectrochemical performance of porous TiO_2/graphene nanocomposite films. *Materials Letters* **2018,** *213*, 109-113.

17. Xu, Y.-Y.; Lu, S.-Q.; Zheng, Y.-Z.; Fang, H.-B.; Tao, X.; Chen, J.-F., Visible-light driven C@TiO_2 porous films: Enhanced photoelectrochemical and photoelectrocatalytic performance. *Catalysis Communications* **2015,** *69*, 63-67.

18. Liu, C.; Chen, L.; Su, X.; Chen, S.; Zhang, J.; Yang, H.; Pei, Y., Activating a TiO_2/$BiVO_4$ Film for Photoelectrochemical Water Splitting by Constructing a Heterojunction Interface with a Uniform Crystal Plane Orientation. *ACS Applied Materials & Interfaces* **2022,** *14* (1), 2316-2325.

19. Cui, W.; Bai, H.; Shang, J.; Wang, F.; Xu, D.; Ding, J.; Fan, W.; Shi, W., Organic-inorganic hybrid-photoanode built from NiFe-MOF and TiO_2 for efficient PEC water splitting. *Electrochimica Acta* **2020,** *349*, 136383.

20. Xu, R.; Zhu, D.; Du, K.; Cui, D.; Feng, H.; Hao, W.; Tian, D.; Du, Y., Role of surface wettability in photoelectrocatalytic oxygen evolution reactions. *Materials Today Energy* **2022,** *25*, 100961.

21. Hou, L.; Bu, Q.; Li, S.; Wang, D.; Xie, T., Ni_3S_2-Decorated TiO_2 nanotube arrays as effective photoanodes for photoelectrochemical water splitting. *RSC Advances* **2016,** *6* (101), 99081-99087.

22. Wang, G.; Xiao, X.; Li, W.; Lin, Z.; Zhao, Z.; Chen, C.; Wang, C.; Li, Y.; Huang, X.; Miao, L.; Jiang, C.; Huang, Y.; Duan, X., Significantly Enhanced Visible Light Photoelectrochemical Activity in TiO_2 Nanowire Arrays by Nitrogen Implantation. *Nano Letters* **2015,** *15* (7), 4692-4698.

23. Wang, N.; Wang, J.; Liu, M.; Ge, C.; Hou, B.; Liu, N.; Ning, Y.; Hu, Y., Preparation of FeS_2/TiO_2 nanocomposite films and study on the performance of photoelectrochemistry cathodic protection. *Scientific Reports* **2021,** *11* (1), 7509.

24. Xue, D.; Luo, J.; Li, Z.; Yin, Y.; Shen, J., Enhanced Photoelectrochemical Properties from Mo-Doped TiO_2 Nanotube Arrays Film. *Coatings* **2020,** *10* (1), 75.